Colloidal and chemical stabilities of iron oxide nanoparticles in aqueous solutions: the interplay of structural, chemical and environmental drivers

Edwige Demangeat, Mathieu Pédrot, Aline Dia, Martine Bouhnik-Le Coz,
Fabien Grasset, Khalil Hanna, M. Kamagaté, Francisco Cabello-Hurtado

Environmental Science
Nano

Accepted Manuscript

Volume 3 | Number 1 | February 2016 | Pages 1–224

Environmental
Science
Nano

rsc.li/es-nano

ISSN 2051-8153

ROYAL SOCIETY
OF CHEMISTRY

PAPER
Joel A. Pedersen et al
Formation of supported lipid bilayers containing phase-segregated
domains and their interaction with gold nanoparticles

175 YEARS

ROYAL SOCIETY
OF CHEMISTRY

Environmental significance statement

Amongst engineered nanoparticles, iron oxide nanoparticles (IONPs) appear particularly relevant toward the environment. Indeed, considering their potential uses in environmental fields (water and soil depollution, agrochemistry, etc.), it becomes critical to determine their behavior and fate in the environment. Their stability and reactivity are dependent upon the environmental parameters, and both intrinsic and surficial properties of IONPs. This work focused on the aggregation behavior of IONPs (especially magnetite, maghemite, hematite), their chemical transformation (oxidation of magnetite) and the impact of a surface coating that mimic natural interactions possibly occurring in the environment. Understanding these interactions and transformations will thus bring key insights regarding the mobility, bioavailability and chemical reactivity of IONPs in prevailing environmental conditions.

Environmental Science: Nano

ARTICLE

Colloidal and chemical stabilities of iron oxide nanoparticles in aqueous solutions: the interplay of structural, chemical and environmental drivers

E. Demangeat,[a] M. Pédrot,[a] A. Dia,[a] M. Bouhnik-le-Coz,[a] F. Grasset,[b] K. Hanna,[c] M. Kamagate[c] and F. Cabello-Hurtado[d]

Nanoparticle (NP) stability in aqueous environments is dependent upon many parameters including environmental conditions, NP concentrations as well as NP intrinsic characteristics. In this study, the effects of pH and surface modifications on the colloidal and chemical stabilities of nanosized magnetite (Fe_3O_4), maghemite (γ-Fe_2O_3) and hematite (α-Fe_2O_3) are investigated. Because changes in surface charge affect the size distribution of NP, pH plays a key role in driving the colloidal stability. More NP aggregation is observed at pH values close to the pH of zero point of charge (pHzpc). Coating of magnetite with humic acid (HA) and phosphatidylcholine (PC) affects the electrostatic interactions and then the colloidal behavior of NP. The rapid transformation of magnetite into maghemite through air oxidation results in significant modification of both surface charge and specific surface area of NP. Because the maghemite almost exclusively formed μm-scale aggregates, the colloidal stability of magnetite is expected to be hindered in oxic environments. For hematite, the particle size distribution data emphasize the influence of both pH and intrinsic surface properties in colloidal stability. These findings may have strong implications for an accurate prediction of the transformation and mobility of Fe-nanoparticles under environmentally relevant conditions and thus their fate in nature.

Introduction

Understanding the prevailing processes controlling chemical exchanges at soil/water interfaces is an environmental priority with regards to their impacts on both ecosystems and soil services, as well as water resources. Iron (Fe) oxides are ubiquitous minerals constituent of soils, sediments, aquifers and geological materials[1, 2]. Their origin is also anthropogenic as they are increasingly used in various fields such as for industrial, medical and environmental purposes[3-6]. Iron oxides nanoparticles (NP) respective stability, specific surface area, porosity, dissolution rate as well as transformation kinetics are controlled by their mineral structure and determine their fate and behaviour in the environment[7]. Amongst them, iron oxide nanoparticles, which also occur as ubiquitous phases in both soils and waters, play a critical role in the chemical dynamics resulting from environmental condition changes since nano minerals are highly reactive[8, 9]. In the natural conditions, only a small fraction of engineered iron oxide NP persists in its original form[10]. Biotransformation, oxidation/reduction, dissolution, precipitation, sorption and photochemical transformation may occur amongst other biogeochemical driven processes[11, 12]. In turn, this transformation can affect the aggregation, mobility,

biointeractions, uptake and fate of iron oxide NP in the environment as well as their impacts on the living environment[13].

Engineered iron oxide NP will become new tools for the treatment of contaminated waters and soils[14, 15]. As compared to conventional macroscale materials, nanomaterials exhibit a high surface-to-volume ratio and high reactivity. Thus, their colloidal size may give them high mobility in porous media and their properties allow them to be particularly suitable for the treatment of contaminated soils or aquifers. Iron oxide NP are involved in (i) the dechlorination of organic solvents (CCl_4, C_2Cl_4), (ii) the detoxification of pesticides (such as Lindane, DDT), (iii) the transformation of fertilizers (NO_3^-), and (iv) the immobilization of metals and metalloids (As, Pb, Cr, etc.)[16-18]. If remediation projects using iron oxide NP are currently focused on local-scale pollution, a scale change is initiated to act against diffuse pollution. Moreover, their use in nano-agrochemistry could be developed in the years ahead and would represent an intentional diffuse source of iron oxide NP within the environment[19]. A widespread use of iron oxide NP for *in situ* remediation or in agriculture also raises the question of their environmental compatibility.

Amongst engineered iron oxide NP of environmental concern, magnetite (Fe_3O_4), maghemite (γ-Fe_2O_3) and hematite (α-Fe_2O_3) are popular engineered iron oxide NP because of their biocompatibility and safety towards living organisms under certain conditions[20-22]. In particular, magnetite has shown an outstanding applicability in many research areas (e.g., semiconductor, magnetic resonance imaging, pigment, biomedicine, drug delivery, heterogeneous

a. *Univ. Rennes, CNRS, Géosciences Rennes - UMR 6118 – F- 35000 Rennes, France*
b. *Univ. Rennes, CNRS-Saint-Gobain-NIMS-UMI LINK 362-J-305-044, Tsukuba, Japan*
c. *Univ. Rennes, ENSCR- CNRS, ISCR (Institut des Sciences Chimiques de Rennes) - UMR 6226 F-35000 Rennes, France*
d. *Univ. Rennes, CNRS, Ecobio - UMR 6553 - F-35000 Rennes, France*

52 catalysis, and environmental remediation)[23, 24, 25] due to its unique 53 magnetic properties and easy manipulation for control of 54 morphologies, particle size, and Fe^{II}/Fe^{III} stoichiometry[26, 27]. 55 However, determination of magnetite compositions which is highly 56 sensitive to the preparation conditions is not a trivial task, 57 particularly for nanoscale particles with a higher surface-to-volume 58 ratio. Magnetite compositions range, without modification of the 59 crystal structure, from that of stoichiometric Fe_3O_4, with 8 Fe^{3+} ions 60 in tetrahedral and 8 Fe^{2+} + 8 Fe^{3+} ions in octahedral sites, to that of 61 maghemite γ-$Fe^{III}_2O_3$ (considered as an extreme example of a non-62 stoichiometric magnetite) with only Fe^{3+} ions in both tetrahedral 63 and octahedral sites. As compared to these iron oxides, hematite 64 has only one type of cation, Fe^{3+} in its structure[28, 29].

65 In aqueous solution, iron oxides (IO) are amphoteric solids that 66 acquire a surface charge in the protonation and deprotonation 67 reactions of Fe-OH surface sites. The ensuing electrostatic, steric or 68 combined stabilization layers that develop at the surface of the 69 particles are significant in driving iron oxide NP colloidal stability[30]. 70 The interfacial equilibrium at the surface of iron oxide NP is thus 71 affected by the adsorption and desorption of the various 72 constituents of the soil and soil solution in addition to the solution 73 pH[31, 32]. The surface charge of iron oxide NP is also dependent upon 74 their own structural organization such as isomorphic substitutions, 75 which give iron oxide NP permanent charges.

76 As part of the Natural Organic Matter (NOM) occurring within 77 soils and waters, macromolecular polyfunctional humic acid (HA), 78 which displays a particular affinity for metal ions and their various 79 acidic functional groups (carboxylic, phenolic, carbonyl), favours the 80 formation of surface complexes on the Fe-OH sites of iron oxides 81 via chemisorption[33]. As a consequence, interactions between iron 82 oxide NP and HA should be further investigated. Several studies 83 have shown that, in aqueous solution, the HA coating on iron oxide 84 NP likely imparts a negative charge to the nanoparticle surfaces, 85 increasing their surface potential and the ensuing propensity to 86 stabilize iron oxide NP against aggregation[34-36]. Nevertheless, Hadju 87 et al.[37] demonstrated that coating magnetite with HA could either 88 foster or hinder Fe_3O_4-NP colloidal stability depending on the 89 amount of HA present at the mineral surfaces. Other natural 90 constituents such as amphiphilic phospholipids (integral major 91 component of cell membranes) likely affect iron oxide NP stability. 92 Using phospholipids as a coating on pyrite surfaces, Hao et al.[38] 93 demonstrated that surface-bound lipids inhibit the iron core from 94 oxidizing, even in the presence of bacteria, by forming a 95 hydrophobic pocket[38, 39]. In addition, several authors have shown 96 that a phospholipid coating likely decreases nanoparticle size 97 dispersion and favours narrow-sized nanoparticles[40, 41]. 98 Furthermore, the instability of magnetite in air causes NP to 99 undergo a partial oxidation to maghemite (γ-Fe_2O_3), ending up with 100 a core-shell structure in which the thickness of the oxidized layer is 101 a function of the particle size[42, 43]. This phase transformation 102 directly affects the surficial properties and internal characteristics 103 of NP, which are deeply involved in driving iron oxide chemical 104 stability and reactivity[44, 45].

105 In the environment, soils and soil solutions are prior interfaces 106 for iron oxide NP interactions[46] occurring at mineral surfaces and in 107 water. In addition to particle interactions, NP are prone to various 108 chemical and physical modifications which foster the complexity of 109 the reactions and likely affect both NP stability and reactivity. 110 Electrostatic, steric or combined electrosteric forces can result from 111 these interactions and promote repulsive forces whereas Van der 112 Waals and magnetic dipolar interactions foster attraction between 113 particles that likely aggregate. The intrinsic physicochemical 114 properties of iron oxide NP (size, shape, surface area, chemistry, 115 superparamagnetism, etc.), their ensuing high reactivity, together 116 with the surrounding solution composition (dissolved species, pH, 117 ionic strength, nanoparticle concentration), are the main drivers of 118 iron oxide NP chemical and colloidal stability in aqueous media[47, 48].

119 Considering the geochemical, biological and technological 120 significance of iron oxide NP[49], understanding the mechanisms of 121 their stability may turn out to be relevant to unravel the fate and 122 behaviour of iron oxide NP in the environment as well as their 123 impacts on living organisms. Therefore, the aim of this work is to 124 investigate the dual colloidal and chemical stability of magnetite NP 125 in order to (i) understand the effects of their intrinsic properties 126 (size, morphology, surface chemistry) and those of the 127 environmental drivers (especially the effect of pH) on their 128 aggregation state, (ii) assess the oxidation kinetics of magnetite, (iii) 129 investigate the link between colloidal and chemical stability of NP, 130 as well as (iv) identify the resulting environmental impacts. 131 Hematite has also been studied to better understand the impact of 132 intrinsic structural properties on iron oxide NP colloidal stability as 133 the structure of hematite differs from both magnetite and 134 maghemite. Indeed hematite NP size and morphology as well as 135 internal crystal structure, generally confer a higher stability and 136 crystallinity to hematite. Last, the method we chose to study the 137 iron oxide NP aggregation state allowed us to study their size 138 distribution over a wide range of sizes (that spread from one tenth 139 of a nm to µm-scale aggregates) which allowed us to determine NP 140 behavior in a context comparable to those observed in natural 141 waters.

Experimental

Iron oxide nanoparticles and coated magnetite NP

144 **Synthesis of bare iron oxide NP.** Magnetite (Fe_3O_4) was 145 prepared by the co-precipitation of iron salts according to the 146 modified literature procedure [50, 51]. In brief, $FeCl_2.4H_2O$ (1.988 g) 147 and $FeCl_3.6H_2O$ (5.406 g) were dissolved in 5 mL HCl (2 M) and 20 148 mL H_2O, respectively, and then mixed with magnetic stirring to 149 obtain an iron solution with a molar ratio of Fe(II)/Fe(III) = 0.5. 150 Magnetite NP were then precipitated by the dropwise addition of 151 the iron salt solution into a 0.7 M $NaOH$-$NaNO_3$ base solution (250 152 mL). The black precipitate was left to settle in anaerobic conditions 153 for a few hours to get rid of the supernatant. Three washings were 154 then conducted in anaerobic conditions with deoxygenated 155 deionized water and 5 10^{-3} M NaCl solution.

156 Maghemite (γ-Fe$_2$O$_3$) was synthesized following the method of
157 Anna et al.[52], through the oxidation of the previously synthesized
158 magnetite by adding 5 wt% NaOCl aqueous solution (16 mL) and
159 sonicating for 2 hours. The solid product was magnetically
160 separated and washed with water.

161 Hematite (α-Fe$_2$O$_3$) was synthesized by the forced hydrolysis of acid
162 Fe(III) salt solutions at 98°C from 0.02 M Fe(NO$_3$)$_3$ following the
163 protocol described in Schwertmann & Cornell (2003)[1].

164 **Coatings with humic acid and phosphatidylcholines.** Fe$_3$O$_4$-NP
165 were coated with HA (Elliott Soil Humic Acid Standard IV) and PC (1,
166 2-bis (10, 12-tricosadiynoyl)-sn-glycero-3-phosphocholine - CAS
167 Registry Number: 76078-28-9) to model a natural surface
168 modification. The coating was carried out by physical interactions
169 between the dissolved organic species (HA and PC) and a
170 concentrated fraction of the Fe$_3$O$_4$-solution. Humic acid (0.2 g) was
171 dissolved in 10 mL NaOH (1 M) and the obtained HA-solution was
172 completed to 56 mL with deionized water. A similar PC-solution was
173 obtained by dissolution in deionized water and ultrasonication.
174 Fourty-four mL of a 6.0 g L^{-1} Fe$_3$O$_4$-NP solution was then added to
175 each organic stock solution and each 100 mL of solution was shaken
176 for 48 hours. At the end of the interaction, five washings were
177 performed to remove the uncoated materials present in the
178 supernatant after centrifugation.

179 **Nanoparticle mass concentration measurement.** The
180 concentration of the iron oxide NP solution was inferred from the
181 ICP-MS measurements of iron on triplicate samples for the iron
182 oxide NP solutions and then recalculated regarding the total
183 theoretical iron content of the minerals. Each NP sample was
184 digested with sub-boiled nitric acid (14.6 M HNO$_3$) at 85°C, and then

209 re-solubilized in 0.37 M HNO$_3$ after complete evaporation before
210 measurement. Major- and trace-element concentrations were
211 determined by ICP-MS (Agilent 7700x), using rhenium and rhodium
212 as the internal standard. The international geostandard SLRS-5 was
213 used to check the validity and reproducibility of the results[53].

215 **Characterization**

216 **Size, morphology and surface properties.** The morphology and
217 individual particle size of Fe$_3$O$_4$, HA-Fe$_3$O$_4$, PC-Fe$_3$O$_4$, γ-Fe$_2$O$_3$ and α-
218 Fe$_2$O$_3$ were determined using High Resolution Transmission
219 Electron Microscopy (HR-TEM) with a JEOL2100F (voltage 200 kV).
220 Specimens were prepared by drop-casting diluted Fe-NP
221 suspensions on 300 mesh Au-grids supported with carbon film.
222 The specific surface area of the iron oxides was determined by
223 multipoint N$_2$–BET (Brunauer Emmett Teller) analysis using a
224 Coulter (SA 3100) surface area analyzer.
225 The pH of zero point of charge was determined by potentiometric
226 titrations, which were conducted with 1 and 2 g L^{-1} of solid at three
227 ionic strengths (10^{-2}, 5.10^{-2}, and 10^{-1} M of NaCl). The suspension
228 was purged with nitrogen gas to remove CO$_2$ in a double-walled
229 Pyrex cell, which was kept at constant temperature by circulating
230 water from thermostat. Titrations were conducted from 4 to 10 by
231 addition of titrant solutions (HCl or NaOH).
232 Synthesized NP were characterized using X-ray powder diffraction
233 (XRD). XRD data were collected with a Johanson monochromator
234 using CuK$_α$ radiation (λ = 1.5406 A). The X-ray diffractograms were
235 found to be identical with the expected oxides.
236 Laser particle size analyses allowed the characterization of the size
237 distribution of magnetite, maghemite, hematite and HA- and PC-
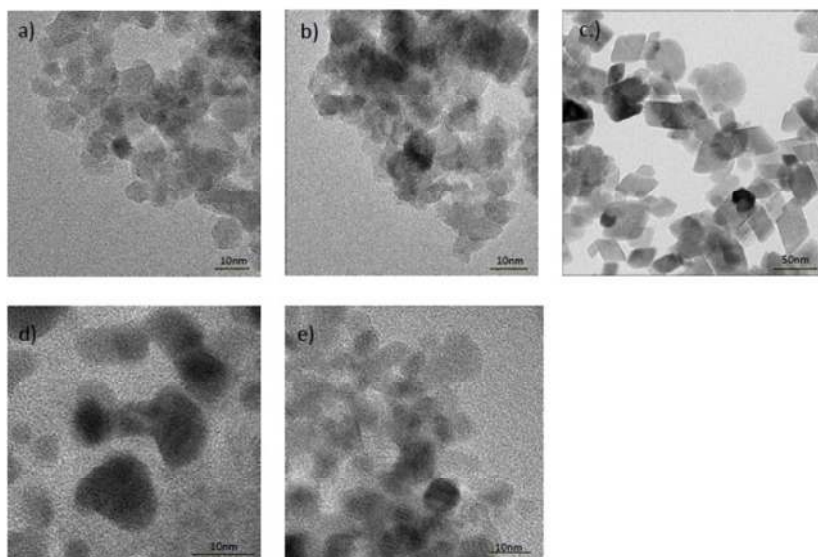
Fig. 1: High Resolution TEM (HRTEM) images of a) Fe$_3$O$_4$, b) γ-Fe$_2$O$_3$, c) α-Fe2O3, d) HA-Fe$_3$O$_4$ and e) PC-Fe$_3$O$_4$

263 264 265 266 267 268 269 270 271 272

NP	TEM (nm)	BET (m² g⁻¹)	pHzpc
Magnetite	7 ± 2	115	5.8
Maghemite	6 ± 2	131	7 - 8.4
Hematite	28 ± 5 39 ± 5	49	8.2

Table 1: Physicochemical properties of a) Fe₃O₄, b) γ-Fe₂O₃ and c) α-Fe₂O₃ obtained from TEM, BET analyses and potentiometric titration.

273 coated magnetite to study the colloidal stability and, conversely, 274 their aggregation behaviour. Assuming measurements on spherical 275 particles, the technique provided sizes amongst the 100 size classes 276 detected, which spread from 0.04 μm to 2500 μm. Analyses were 277 performed by the laser diffraction technique on a Cilas1180 278 analyzer. Measurements were taken on each bare iron oxide (Fe₃O₄, 279 γ-Fe₂O₃ and α-Fe₂O₃) and coated magnetite (HA-Fe₃O₄ and PC-280 Fe₃O₄) at five different pH values (pH = 3, 4, 5, 6, 7.5). Particle size 281 measurements were performed by adjusting obscuration values 282 allowing for an optimal analysis. Then, the pH was equilibrated with 283 HCl and NaOH solutions (0.1 M and 0.1 M to 1.0 M, respectively) 284 until the target pH was reached.

285 **ATR-FTIR.** Attenuated total reflectance-Fourier transform 286 infrared (ATR-FTIR) spectra were recorded in the 780 - 1800 cm⁻¹ 287 region on an IS50 Nicolet spectrometer equipped with a KBr beam 288 splitter and a liquid Nitrogen cooled MCT (Mercury Cadmium 289 Telluride) detector. A nine-reflection diamond ATR accessory 290 (Durasampl*IR* ™, SensIR Technologies) was used for acquiring 291 spectra of wet samples. The resolution of the single beam spectra 292 was 4 cm⁻¹. Prior to ATR-FTIR analyzes, tubes containing coated NP 293 were centrifuged at 4110 RCF for 30 min. Wet mineral pastes were 294 directly and uniformly applied to the diamond ATR crystal then 295 covered with a lid of a flow-through cell to prevent the evaporation 296 of water. ATR-FTIR spectra were then recorded immediately.

297 To monitor potential dissolution of NP, aliquots were collected at 298 each pH value, centrifuged and the supernatants were filtered using 299 5 KDa ultrafiltration cells (from Sartorius) in order to stop NP on the 300 filter. ICP-MS was then performed to measure total iron 301 concentration.

302 **Oxidation kinetics.** A NP suspension (2.5 g L⁻¹), prepared in 303 anoxic conditions, was placed outside the glove box under air 304 ambient environment to monitor the oxidation. The total 305 Fe(II)/Fe(III) ratio in suspension was then analyzed versus time over 306 nine days. For each sampling, two aliquots were placed in an 307 anaerobic chamber: the first aliquot contained bulk solution and 308 the second was filtered (0.2 μm, Whatman). NP suspension was 309 dissolved during 12h using 0.6 N HCl while filtered NP were directly 310 dissolved. Dissolved Fe(II) and Fe(III) concentrations were then 311 determined using the phenanthroline method[54, 55] and the bulk 312 Fe(II) content turned out to be very close to that determined by 313 acid digestion on the filtered solid. The amount of magnetite 314 bound-Fe(II) ([Fe(II)] bound = [Fe(II)]tot − [Fe(II)]aq) was used to 315 calculate the effective Fe(II)/Fe(III) ratio (denoted as (Fe(II)/Fe(III)) 316 bound) in magnetite which was shown to vary with pH, as reported

317 in Cheng et al.[56]. [Fe(II)]tot is the total concentration of Fe(II) in the 318 suspension (solid + solution) and [Fe(II)]aq is the dissolved 319 concentration of Fe(II), measured after filtration (0.2 μm, 320 Whatman) of the magnetite suspension.

321

Results and discussion

### Iron oxide NP physicochemical properties.

HR-TEM analyses provided images to assess the individual sizes and 325 shapes of the nanoparticles (Fig. 1). Magnetite and maghemite 326 oxides both displayed rounded shapes and similar sizes with 327 average diameters of 7 ± 2 nm and 6 ± 2 nm (Table 1), suggesting 328 that the oxidation of magnetite to maghemite did not impact the 329 particle size. Accordingly, BET surface area for maghemite (131 m²g⁻¹) 330 is relatively close to that of magnetite (115 m²g⁻¹) (Table 1). 331 Hematite displayed different morphologies with rhombohedral 332 shapes measuring 28 nm-wide and 39 nm-long on average, with a 333 surface area of 49 m²g⁻¹ (Table 1). No significant changes were 334 reported for neither HA- nor PC-coated magnetite from TEM 335 images, suggesting that the coating process did not modify the 336 morphology of magnetite. Although the surface area was not 337 determined for coated materials, no significant modification is 338 expected, according to previous findings[57].

ATR-FTIR spectroscopy

341 The IR spectrum recorded for of Fe₃O₄, HA-Fe₃O₄- and PC-Fe₃O₄ 342 showed successful coating of HA and PC on magnetite surfaces (Fig. 343 2). In the spectra of HA-Fe₃O₄, the presence of an acid carboxylic 344 group was proven by the vibrational bands at 1410 cm⁻¹ and 1614 345 cm⁻¹ [58-60]. In the spectra of PC-Fe₃O₄, the absorption bands at 1239 346 cm⁻¹, 1088 cm⁻¹ and 970 cm⁻¹ were assigned to the presence of the 347 PO₄³⁻ group, suggesting that PC was coated on the magnetite 348 surface[61, 62].

349

Oxidation kinetics

351 The variation of total Fe(II)/Fe(III) ratio versus time for magnetite 352 suspension exposed to air is characterized by a two-steps' behavior. 353 Over the four first days (0-96 h), a sharp decrease in total
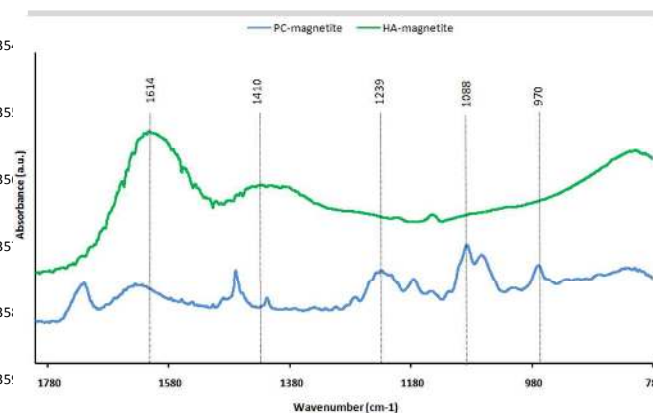
Fig 2: ATR-FTIR spectra of HA-magnetite and PC-magnetite in the range 780-1800 cm⁻¹ obtained from 0.5 g L⁻¹ NP suspensions at pH= 6.
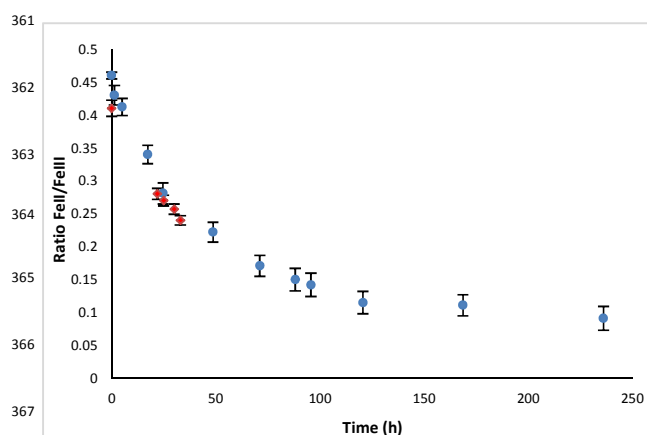
Fig 3: Evolution of the total Fe(II)/Fe(III) ratio (blue circles) and bound Fe(II)/Fe(III) ratio (red diamond) as a function of time. The reaction was performed with 2.5 g L^{-1} magnetite NP at pH = 7.5 in oxic conditions.

Fe(II)/Fe(III) ratio was observed (from 0.46 to 0.09). During this first stage, the bound Fe(II)/Fe(III) ratio was also decreased for magnetite as represented by red symbols in Figure 3. Then, the total Fe(II)/Fe(III) ratio slightly decreased beyond 5 days to reach 0.09 at the end of the experiment (236 h). As expected from the magnetite solubility at pH = 7.5[1], very little difference was observed between the total and bound Fe(II)/Fe(III) ratios.

Aggregation state

To assess the effect of pH and the effects of coating, laser diffraction analyses were performed on each iron oxide (Fe$_3$O$_4$, HA-Fe$_3$O$_4$, PC-Fe$_3$O$_4$, γ-Fe$_2$O$_3$ and α-Fe$_2$O$_3$) at five different pH values. For all experiments, the aggregation state was associated with the size distribution of the NP, which was described by considering the evolution of the sizes (based on number analyses) with the pH, occurrence rate and the polydispersity of the sizes (PDI, size range, mode and mean) of each iron oxide NP.

Effects of pH. The impact of pH on particle size distribution provides valuable information that could be used to distinguish the colloidal stability from the aggregation state of the various NP (Table 2). The different pH-dependent configurations highlighted the role of pHzpc in controlling NP aggregation through electrostatic interactions (Fig. 4). The effect of pH was studied by considering the evolution of the size distributions into four size classes (Fig. 4). The fractions were defined with regards to the most common sizes (representability) and depending on the way they vary with pH. However, it should be noted that fractions are not fully comparable to one another, as they were not spread out equally (i.e. fraction >0.4 µm (µm-scaled size class) as compared to 40-100 nm fraction (nm-scaled sizes)). The full-size distribution diagrams obtained from laser particle analyses as well as the precise occurrence rates (detectors) are provided in the Electronic Supporting Information (ESI).

It is worth noting that the total dissolved iron content was only detected in the magnetite suspension at pH = 3 and pH = 4 (90 and 23 µmol L^{-1} respectively). These values correspond to 1.4 % and 0.4 %, respectively, of the total iron amount in NP suspension. For HA- and PC-magnetite samples, no dissolved iron was detected regardless of the investigated pH.

Magnetite. The NP size distribution displayed two configurations: at pH = 5, 4 and 3, magnetite NP showed colloidal stability as compared to their size distribution at pH = 6 and 7.5. Magnetite size distribution at acidic pH was characterized by a high proportion of small NP (≤0.04 µm), and the occurrence of few dispersed µm-scaled aggregates (with sizes ranging between 1.6 µm and 32 µm). Such distribution allowed a large amount of NP not to sediment, as defined by Buffle et al.[63]. When the pH increased to 6 and 7.5, the number of coarser 100-400 nm and 40-100 nm-sized aggregates increased as the proportion of small aggregates decreased. This is consistent with the measured pHzpc = 5.8 (in accordance with previously published values[4]), since aggregation is commonly favoured at pH close to the pHzpc. Therefore, particles exhibiting negative charges likely formed coarser aggregates when the pH approached the pHzpc because of favorable electrostatic interactions[64].

	Magnetite		HA-Magnetite		PC-Magnetite			Maghemite			Hematite	
pH	6	5	4	3	7.5	5	4	7.5	6	5	7.5	5
Range (µm)	0.04 - 0.4; 1.6 - 32	0.04 - 0.4; 1.6 - 32	0.04 - 18	0.04 - 0.4; 1.1 - 19	0.04 - 0.4; 1.2 - 45	0.04 - 0.4; 1.1 - 40	0.04 - 0.4; 1.6 - 56	0.04 - 0.4; 1.6 - 28	0.04 - 0.4; 1.6 - 28	0.5 - 0.7; 1.1 - 28	0.04 - 6	0.04 - 0.4; 1.1 - 12
Mode (µm)	0.04	0.04	0.04	0.04	0.04	0.04	0.04	0.04	0.04	8	1.4	0.04
Mean (µm)	1.3	0.9	0.4	0.6	1.1	0.8	1.3	4.1	1.1	6.8	1.3	0.5
Median (µm)	0.07	0.04	0.04	0.07	0.07	0.04	0.07	0.2	0.04	7	1.2	0.04
PDI	1.38	2.74	13	5	1.9	3.4	1.3	0.56	2.06	0.72	4.8	7.6

Table 2: Size distribution characteristics of each NP at some typical pH (aggregation state versus colloidal stability). The table shows the size-range, mode, mean size, median value and the PDI (polydispersity index) of magnetite, HA-coated magnetite, PC-coated magnetite, maghemite and hematite. High PDI have values up to 1.0 and very high PDI are up to 2.0.

ARTICLE

Journal Name
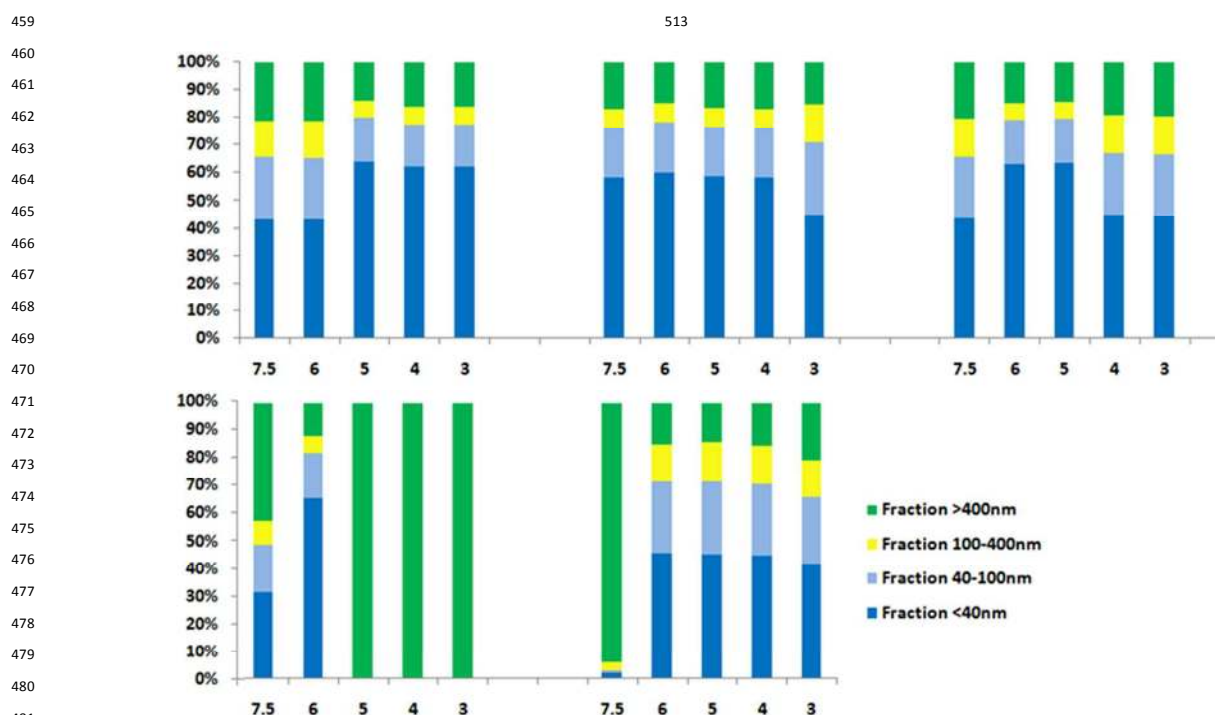
Fig 4: Evolution of four typical size-class (proportion in %) with pH for a) magnetite, b) HA-magnetite, c) PC-magnetite, d) maghemite and e) hematite. Below the histograms, the table displayed the percentages of each fraction for typical pH (3, 4, 5, 6 and 7.5).

HA-Magnetite. HA-magnetite nanoparticles displayed both a continuous size distribution (pH = 4 to pH = 7.5) and a dual size distribution (pH = 3). In both cases, fraction below 0.04 μm was more important but their proportion decreased as the pH decreased from pH = 4 to 3. This decrease was accompanied by a slight increase in 40–100 nm-sized fraction and an increase in the proportion of coarser intermediate 100-400 nm NP size-class, which appeared to be more dependent upon pH than other fractions. The occurrence rate of the coarse aggregate fraction (>0.4 μm and >1.1 μm) remained constant regardless of the pH, hence a lower pH implied a moderated aggregation with small (≤0.04 μm) particles aggregating in only slightly coarser (0.05-0.4 μm) aggregates. Thus in HA-coated iron oxide NP, HA appeared to be an effective organic stabilizer towards iron oxide NP as previously demonstrated[65, 66].

PC-Magnetite. PC-magnetite nanoparticles highlighted two size distribution depending on the pH. At pH = 6 and 5, the size distribution was similar to that of bare magnetite at acidic pH (pH = 3 and pH = 4) where the colloidal stability displayed its maximum. At pH = 7.5, 4 and 3, Fe_3O_4-PC showed a similar size distribution to bare magnetite at pH >6, when it aggregated. When the pH decreased to pH = 4 and pH = 3, small aggregates (≤ 0.04 μm) were still the most common but in a lower proportion which was compensated by a higher amount of the three other coarser size fractions (in order: 40-100 nm; >1.6 μm and 100-400 nm). Although 100-400nm-sized aggregates were still the least common, this fraction was the most sensitive to pH as its proportion more than doubled from pH 6 and 5 to pH 4 and 3.

Maghemite. The size distribution displayed three distinct fractions whose proportions were strongly controlled by the pH. At a weak basic pH (pH = 7.5), the distribution was highly polydispersed and made up of coarse aggregates (>0.4 μm), which spread over a large size range. Maghemite NP displayed colloidal stability at pH = 6 with a size distribution similar to that of magnetite. However, when the pH decreased to a more acidic pH (pH = 5, 4 and 3), small-sized NP and NP aggregates disappeared to form much coarser aggregates with almost exclusively μm-scale sizes (>1 μm). Thus, the maghemite size distribution would be in good agreement with a high pHzpc close to 7.5[67, 68], as it became coarser than at pH = 6, but the high aggregation observed from pH = 3 to 5 suggested the possible implication of parameters other than electrostatic interactions to drive maghemite colloidal stability.

Hematite. The hematite size distribution showed two pH-dependent size distribution patterns. At pH = 7.5, the sizes were continuously distributed with a unique narrow size range composed of coarse homogeneous sizes displaying high polydispersity (multimodal distribution centered on 1.4 μm). When the pH decreased to pH = 6 and lower, the pH drastically modified the hematite size distribution to a more stable aggregation state[69] characterized by a monomodal distribution (0.04 μm) and higher abundance of finer particles (<0.4 μm). In accordance with the hematite pHzpc at pH = 8.2, hematite NP tended to aggregate when the pH reached pH = 7.5.

Effects of coating. The physico-chemical characteristics obtained from the combination of HR-TEM and ATR-FTIR showed

ARTICLE

that HA have been successfully coated onto magnetite NP. According to HR-TEM images, HA coating on magnetite did not affect the original morphology and size of the precursor NP. As the surface modification with HA provided primarily acidic functional groups, the HA-coated magnetite pHzpc likely decreased to a lower pH (pHzpc = 2.3). Accordingly, magnetite-HA promoted colloidal stability from pH = 7.5 to pH = 4 because of repulsive electrostatic interactions. The aggregation observed at pH = 3 - close to the new pHzpc - would then be explained by the lack of negative surface sites to compensate for the protonation induced by the H^+ concentration increase in the aqueous solution. Both HA and bare magnetite evidenced that the proportion of their size- fractions was strongly controlled by the pH, which induced either colloidal stability or aggregation. Nevertheless, HA coating promoted smaller-sized aggregates as well as a narrower size distribution and more homogeneous stable sizes (especially for coarser particles (>0.4 μm)) compared to bare magnetite (Table 2). This enhanced stabilization may stem from a HA steric barrier that helped maintain a space between the particles to prevent the aggregation of NP[70, 71]. Similar to the HA coating, the PC surface modification did not affect the size and morphology of magnetite. Magnetite coated with PC displayed a different colloidal behaviour as compared to bare magnetite. As PC imparted both negative and positive surface groups on the surfaces of the NP (glycerophosphate group, trimethylethanolammonium group), and because of the complex and heterogeneous surface structures that are generated by adsorbed PC[72], PC-coated nanoparticles likely displayed variable colloidal behaviours. As compared to magnetite, PC-NP showed similar size proportions and repartition although the magnetite-PC coarse fraction displayed a few large aggregates (hence its wider size range, see Table 2) regardless of the pH. PC-NP were thus probably able to form highly contrasted structures (according to their size) suggesting that PC-coated magnetite did not entirely depend on electrostatic interactions but also on steric forces[72].

Effects of iron oxide intrinsic physicochemical properties. The oxidation of magnetite (Fe_3O_4) to maghemite (γ-Fe_2O_3) did not change morphology and particle size. Maghemite still displayed a higher surface area (131 m^2 g^{-1}) than magnetite (115 m^2 g^{-1}) and oxidized NP very likely yielded intrinsic compositional differences. These modifications probably resulted in a higher surface potential thereby explaining the variable size distributions observed as the pH changed. Maghemite NP aggregation was favoured at acidic pH (equal or below 5), which would be in good agreement with their high surface potential. Indeed, the tendency to form large aggregates at these pH values likely resulted from a high energetic barrier that had to be overcome at the mineral surfaces[73]. Indeed, increasing NP surface to volume ratio leads to a higher surface energy which induces aggregation between particles. As hematite displayed a much lower surface area, the higher colloidal stability observed over a wide pH range may result from a lower energetic barrier at the surface of the particles in accordance with NP having a relatively lower surface potential. Hematite stability would thus be related, in part, to its smaller surface area and surface potential. However, the typical aggregation behaviour of hematite NP displaying coarse aggregates with homogeneous sizes suggests that other mechanisms are involved at basic pH. Further investigations are thus needed to fully assess iron oxide NP colloidal stability[74-76].

Environmental perspectives. Aggregation and stabilization have significant effects on the mobility, reactivity and environmental fate of NP. Once released in surface waters, unstable particles tend to agglomerate, sediment or flocculate or they preferentially adsorb onto bigger particles or surfaces[77]. As a result, aggregated NP that form larger colloids with a possible smaller surface area are less easy to transport and do not get through the soil as easily as smaller particles[78]. As aggregated NP become less mobile, they may become more ineffective in acting as nutrient carriers[79]. It is also more difficult for these colloids to be taken up by plants and living organisms as they are less soluble than their smaller counterparts[80]. The dissolution of NP induces the mobilization of ions which are likely complexed with molecules that foster their absorption by plants and animals. In addition, depending on their concentration and speciation as well as on the physiology of the organism that absorbs it, metal atoms or ions can be either positive nutrients or toxic elements. On the other hand, aggregation may directly affect NP toxicity towards living organisms since smaller NP have been shown to penetrate the cell walls of certain species more easily[81, 82]. Considering the pH effect, the physicochemical properties of the soil solution have to be considered in order to accurately assess the fate of NP in the environment. NP intrinsic properties, such as their surface chemistry, are also of prime importance since they are involved in both electrostatic and steric interactions, which may impact their dispersion, bioavailability and biocompatibility[83]. In natural waters and surficial aerobic environments, NP likely undergo many surficial modifications and become embedded in matrixes or functionalized with specific molecules[84]. As a result, these attached molecules can both passivate and/or confer their own properties to mineral surfaces; e.g. polyanionic HA coating on magnetite, resulting in a lower pHzpc and enhanced colloidal stability. In addition, HA coating - as well as PC covering - might passivate iron oxide NP surfaces to yield a steric barrier that prevents Fe leakage from mineral surfaces and the ageing of the magnetic core by oxidation. HA, which are ubiquitous in most aquatic systems, display a specific affinity for iron oxide NP as well as trace elements and therefore HA-iron oxide NP complexed structures may also enhance ETM adsorption to NP. However, although natural coatings demonstrated improved iron oxide NP stability and reactivity, their effects depend upon the amount and chemical composition of the substances[4]. The rapid oxidation of magnetite into maghemite is important since iron plays an active redox catalytic role in many energy transfer and electron transfer processes[85-87]. The iron oxide redox state also plays a key role in specific anaerobic environments where Fe(II) and Fe(III) are used as energetic catalysts for bacteria[88, 89]. Finally, the transformation of magnetite into maghemite is also relevant considering its adsorption capacity towards environmental compounds[90]. Several questions are raised from these environmental considerations, especially, what are the impacts of these modifications regarding iron oxide NP reactivity?

Conclusions

The pH appears to be a key driver in controlling iron oxide NP colloidal behaviour as resulting from protonation and deprotonation reactions of surface hydroxyl-groups. Surface modifications also implied considerable effects on iron oxide NP colloidal stability as they promoted electrostatic interactions. In contrast to PC, HA was shown to be particularly efficient in enhancing magnetite colloidal stability. Magnetite seems to be highly unstable in aerobic conditions. The oxidation of magnetite into maghemite modified its surface chemistry and surface area, and these modifications resulted in higher aggregation at most pH values. Compared to maghemite, hematite appeared to be less sensitive to pH and displayed a lower surface area and surface potential. Both hematite and maghemite displayed high aggregation size distributions at different pH values.

Considering the widespread use of iron oxide NP and their subsequent release in the environment, their fate and behaviour in soils and natural waters raise many environmental questions not only in terms of their possible impacts on living organisms but also for their mobility and fate in ecosystems. Therefore, more attention should be paid for the understanding of colloidal and chemical stabilities of iron oxide NP as it is likely involved in many major interactions within the environment.

Acknowledgements

References

1   R. M. Cornell and U. Schwertmann, 2nd edition, http://trove.nla.gov.au/version/36973177, 2003, Edited by Wiley-VCH, 664p.

2   M. F. Hochella Jr, S. K. Lower, P. A. Maurice, R. L. Penn, N. Sahai, D. L. Sparks and B. S. Twining, *Science*, 2008, **139,** 1631.

3   A. Afkhami, M. Saber-Tehrani and H. Bagheri, *Desalination*, 2010, **263**, 240.

4   M. A. Ahmed, S. M. Ali, S. I. El-Dek and A. Galal, *Materials Science and Engineering B,* 2013,**178**, 744.

5   A. K. Gupta and M. Gupta, *Biomaterials,* 2005,**26**, 3995.

6   S. Laurent, J.-L.Bridot, L. Van der Elst and R. N. Muller, *Future Medicinal Chemistry,* 2010, **2(3)**, 427.

7   H. Guo and A. Barnard, *Journal of Materials Chemistry A*, 2013, **1**, 27.

8   M. Schindler and M. F. Hochella Jr., *Geology*, 2016, **44**, 515.

9   S. C. Löhr, D. T. Murphy, L. D. Nothdurft, R. Bohlar, S. Piazolo and C. Siegel, *Geochimica and Cosmochimica Acta*, 2017, **200**, 25.

10   C. W. Isaacson, M. Kleber and J. A. Field, *Environmental Science & Technology*, 2009, **43**,6463.

11   B. Nowack and T.D. Bucheli, *Environmental Pollution*, 2007, **150**, 5.

12   M. Auffan, J. Rose, J.-Y.Bottero, G. V. Lowry, J.-P.Jolivet and M.-R.Wiesner, *Nature Nanotechnology*, 2009, **4**, 634.

13   G. V. Lowry, K. B. Gregory, S. C. Apte and J. R. Lead, *Environmental Science & Technology*, 2012, **46**, 6893.

14   S. C. N. Tang, I. and M. C. Lo, *Water Research*, 2013, **47**, 2613.

15   M. Vitkova, S. Rakosova, Z. Michalkova, M. Komarek, *Journal of Environmental Management*, 2017, **186**, 268.

16   P. N. Dave and L. V. Chopda, *Journal of Nanotechnology*, 2014, **2014**, 1.

17   A. Aftabtalab, H. Sadabadi, CH. Shilpa Chakra, K. V. Rao, S. Shaker and E. Privilege Mahofa, *International Journal of Scientific & Engineering Research*, 2014, **5(1)**,1419.

18   S. R. Chowdhury and E. K. Yanful, *Journal of Environmental Management*, 2013, **129**, 642.

19   L. R. Khot, S. Sankaran, J. M. Maja, R. Ehsani and E. W. Schuster, *Crop Protection*, 2012, **35**, 64.

20   E. Navarro, A. Baun, R. Behra, N. B. Hartmann, J. Filser, A-J.Miao, A. Quigg, P. H. Santschi and L. Sigg, *Ecotoxicology*, 2008,**17**, 372.

21   A. Valdiglesias, N. Fernandez-Bertolez, G. Kiliç, C. Costa, S. Costa, S. Fraga, M. J. Bessa, E. Pasaro, J. P. Texeira and B. Laffon, *Journal of Trace Elements in Medicine and Biology*, 2016, **38**, 53.

22   R. Podila and J. M. Brown, *Journal of Biochemical and Molecular Toxicology*, 2013, **27(1)**, 50.

23   W. Wu, Z. Wu, T. Yu, C. Jiang and Woo-Sik Kim, *Sci. Technol. Adv. Mater*., 2015, **16**, 023501.

24   O. Veiseh, J. W. Gunn, M. Zhang, Advanced Drug Delivery Review, 2010, **62**, 304.

25   Y. Ju-Nam and J. R. Lead, *Science of the Total Environment*, 2008, **400**, 414.

26   A-H. Lu, E.L. Salabas and F. Schüt, Angew. Chem. Int. Ed., 2007, **46**, 1244.

27   D. Maity and D.C. Agrawal, *Journal of Magnetism and Magnetic Materials*, 2007, **308**, 46.

28   M. M. Can, M. Coskun and T. Firat, *Journal of Alloys and Compounds*, 2012, **542**, 241.

29   A. Lassoued, M. S. Lassoued, B. Dkhil, A. Gadri and S. Ammar, *Journal of Molecular Structure*, 2017, **1141**, 99

30   S. C. Pang, S. F. Chin and M. A. Anderson, *Journal of Colloid and Interface Science*, 2007, **311**, 94.

31 L. Peng, P. Qin, M. Lei, Q. Zeng, H. Song, J. Yang, J. Shao, B. L. and J. Gu, *Journal of Hazardous Materials*, 2012,**209-210**,193.

32 E. Tombacz, Z. Libor, E. Illès, A. Majzik and E. Klumpp, *Organic Geochemistry*, 2004, **35**, 257.

33 A. M. Vindedahl, J. H. Strehlau, W. A. Arnold and R. L. Penn, *Environmental Science: Nano, Critical Review*, 2016, **3**, 1.

34 M. Baalousha, *The Science of the Total Environment*, 2009, **407**, 2093.

35 E. Illes and E. Tombacz, *Journal of Colloid and Interface Science,* 2006, **295**,115.

36 E. Tombacz, I.Y. Toth, D. Nesztor, E. Illés, A. Hadju, M. Szekeres and L. Vékas, *Colloids and Surfaces A: Physicochemical and Engineering Aspects*, 2013,**435**, 91.

37 A. Hajdú, E. Illés, E. Tombácz and I. Borbáth, *Colloids and surfaces A: Physicochemical and Engineering Aspects*, 2009, **347**, 104.

38 J. Hao, C. Cleveland, E. Lim, D. R. Strongin and M. A. A. Schoonen, *Geochemical Transactions*, 2006, **7:8**, 1.

39 X. V. Zhang, T. A. Kendall, J. Hao, D. R. Strongin, M. A. A. Schoonen and S. T. Martin, *Environmental Science & Technology*, 2006, **40**, 1511.

40 J. Giri, S. G. Thakurta, J. Bellare, A. K. Nigam and D. Bahadur, *Journal of Magnetism and Magnetic Materials*, 2005, **293**, 62.

41 S. Chatterjee, M. Krikorian, H. D. Gafney and B. Gersten, *Material Research Society*, 2011, **1061**, MM09-08.

42 R. Frison, G. Cernuto, A. Cervellino, O. Zaaharko, G. M. Colonna, A. Guagliardi and N. Masciocchi, *Chemistry of Materials*, 2013, **25**, 4820.

43 U. S. Khan, Amanullah, A. Manan, N. Khan, A. Mahmood and A. Rahim, *Material Science-Poland*, 2015, **33(2)**, 278.

44 I. Nedkov, T. Merodiiska, L. Slavov, R.E. Vandenberghe, Y. Kusano and J. Takada, *Journal of Magnetic Materials*, 2006, **300**, 358.

45 H. Shokrollahi, *Journal of Magnetism and Magnetic Materials*, 2017, **426**, 74.

46 L. Charlet G. Morin, J. Rose, Y. Wang, M. Auffan, A. Burnol and A. Fernandez-Martinez, *ComptesRendus Geoscience*, 2011, **343**, 123.

47 L. Chekli, S. Phuntsho, M. Roy, E. Lombi. E. Donner and H. K. Shon, *Water Research*, 2013, **47**, 4585.

48 W. Li, J. Wu, C. Kim and J. D. Fortner, *Environmental Science &Technology*, 2014, **48(20)**, 11892.

49 A. Navrotsky, L. Mazeina and J. Majzlan, *Science*, 2008, **319**, 1635.

50 R. Massart, *IEEE Transactions on Magnetics*, 1981, **17**,1247.

51 S. E. Khalafalla and G. W. Reimers, *IEEE Transactions on Magnetics*, 1980, **16(2)**, 178.

52 Z. B. Anna, B. Patricyja, J. Petr, E. Petrovsky, B. Pavel, H. Daniel, *Colloids and Surfaces B: Biointerfaces,* 2016, **141**, 389.

53 D. Yeghicheyan, C. Bossy, M. Bouhnik Le Coz, C. Douchet, G. Granier, A. Heimburger, F. Lacan, A. Lanzanova, T. C. C. Rousseau, J.L. Seidel, M. Tharaud, F. Candaudap, J. Chmeleff, C. Cloquet, S. Delpoux, M. Labatut, R. Losno, C. Pradoux Y. Sivry and J. E. Sonke, *Geostandards and Geoanalytical Research*, 2013, **37(4)**, 449.

54 C. A. Gorski and M. M. Sherer, *American Mineralogist*, 2010, **95**, 1017.

55 P. Komadel and J. W. Stucki, *Clays and Clay Minerals*, 1988, **36(4)**, 379.

56 W. Cheng, R. Marsac and K. Hanna, *Environ. Sci. Technol*., 2018, **52 (2)**, 473.

57 J. Lohdia, G. Mandarano, N. J. Ferris, P. Eu and S. F. Cowell, *Biomedical Imaging and Intervention Journal*, 2010,**6(2)**, 1.

58 H. Niu, D. Zhang, S. Zhang, X. Zhang, Z. Meng and Y. Cai, *Journal of Hazardous Materials*, 2011, **190**, 559.

59 J.-F. Liu, Z.-S. Zhao and G.-B.Jiang, *Environmental Science & Technology*, 2008, **42**, 6949.

60 S. Koesnarpadi, S. J. Santosa, D. Siswanta and B. Rusdiarso, *Procedia Environmental Sciences* 30 (2015, 103.

61 S. Debnath, D. B. Hausner, D. R. Strongin and J. Kubicki, *Journal of Colloids and Interface Sciences*, 2010, **341**, 215.

62 Q.-C. Le, M.-H. Ropers, H. Terrisse and B. Humbert, *Colloids and Surfaces B: Biointerfaces*, 2014, **123**, 150.

63 J. Buffle, K. Wilkinson, S. Stoll, F. Montserrat, Z. Jingwu, *Environmental Science & Technology*, 1998, **32(19)**, 2899.

64 A. Kraynov and T. E. Müller, In *Applications of Ionic Liquids in Science and Technology*, 2011, Edited by Prof. S. Handy (516 pages), 235.

65 M. Pédrot, A.L. Boudec, M. Davranche, A. Dia, O. Henin, *Journal of Colloid and Interface Science*, 2011, **359**, 75.

66 D. Palomino and S. Stoll, *Journal of Nanoparticle Research*, 2013, **15(2)**, 1428.

67 N. Fauconnier, J. N. Pons, J. Roger and A. Bee, *Journal of Colloid and Interface Science*, 1997,**194**, 427.

68 L. Vayssieres, *J. Phys. Chem. C*, 2009, **113**, 4736.

69 K. Shimizu, S. V. Sokolov and R. G. Compton, *Colloid and Interface Science Communications*, 2016, **13**, 19.

70 S. Ghosh, W. Jiang, J. D. McClements and B. Xing, *Langmuir*, 2011*,* **27**, 8036.

71 S. F. Meideros, J. O.C. Filizzola, V. F.M. Fonseca, P. F.M. Oliveira, T. M. Silva, A. Elaissari and A. M. Santos, *Materials Letters*, 2015, **160**, 522.

72 R. Michel and M. Gradzielski, *International Journal of Molecular Science*s, 2012, **13**, 11610.

73 K. A. D. Guzman, M. P. Finnegan and J. F. Banfield, *Environmental Science & Technology*, 2006, **40**, 7688.

74 M. D. Carvalho, F. Henriques, L. P. Ferreira, M. Godinho and M. M. Cruz, *Journal of Solid State Chemistry*, 2013,**201**, 144.

75 E. Alp and N. Aydogan, *Colloids and Surfaces A: Physicochemical and Engineering Aspects*, 2016, **510**, 205.

76 D. Dickson, G. Liu, C. Li, G. Tachiev and Y. Kai, *The Science of the Total Environment*, 2012, **429**, 170.

77 A. M. Badawy, A. A. Hassan, K. G. Scheckel, M. T. Suidan and T. M. Tolymat, *Environmental Science and Technology*, 2013, **47**, 4039.

78 M. Komarek, A. Vanek and V. Ettler, *Environmental Pollution*, 2013, **172**, 9.

ARTICLE

79 C. Claudio, E. di Iorio, Q. Liu, Z. Jiang, V. Barron, *Journal of Nanoscience and Nanotechnology*, 2017, **17(7)**, 4449.

80 I. A. Mudunkotuwa and V. H. Grassian, *Journal of Environmental Monitoring*, 2011, **13(5)**, 1135.

81 J. Bauman, J. Köser, D. Arndt and J. Filser, *The Science of the Total Environment*, 2014, **484**, 176.

82 K. Powers, M. Palazuelos, B. M. Moudgil and S. M. Roberts, *Nanotoxicology*, *2007,***1 (1)**, 42.

83 R. K. Das, S. K. Brar and M. Verma, *Trends in Biotechnology*, 2016, **34(6)**, 440.

84 D. Lin, S. D. Story, S. L. Walker, Q. Huang, W. Liang and P. Cai, *Environmental Pollution*, 2017, **228**, 35.

85 K. S. Siddiqi, A. ur Rahman, Tajuddin and A. Husen, *Nanoscale Research Letters*, 2016, **11**, 498.

86 H. Wu, J. J. Yin, W. G. Wamer, M. Zeng and Y. M. Lo, *Journal of Food and Drugs Analysis*, 2014, **22**, 86.

87 S. K. Chaudhuri, J. G. Lack, J. D. Coates, *Applied and Environmental Microbiology*, 2001, **67**, 2844.

88 M. Posfai, T. Kasama, E. T. Simpson, R. K. K. Chong and R. E. Dunin-Borkowski, *ActaCrystallica*, 2006**, 62**, 39.

89 J.-Y. Bottero, M. Auffan, J. Rose, C. Mouneyrac, C. Botta, J. Labille, A. Masion, A. Thill and C. Chaneac, *ComptesRendus Geoscience*, 2011, **343**, 168.

90 M. Davranche, A. Dia, M. Fakih, B. Nowack, G. Gruau, G. Ona-Nguema, P. Petitjean, S. Martin and R. Hochreutener, *Chemical Geology*, 2013,**335**, 24.